Deep–Sea Research I 230 (2026) 104709

Contents lists available at ScienceDirect

Deep-Sea Research Part I

journal homepage: www.elsevier.com/locate/dsri

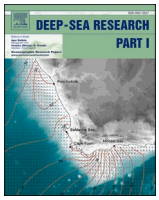

Seafloor erosional processes within the Rio Grande Rise: Integrated results from past scientific expeditions

Gabriel Tagliaro [a,*], Alexandre Henrique Ferraz [a], Raylla Souza Silva [a], Christian Millo [a], Renata Regina Constantino [b], Bramley J. Murton [c], Luigi Jovane [a]

[a] Instituto Oceanográfico, Universidade de São Paulo, Brazil
[b] Instituto de Astronomia, Geofísica e Ciências Atmosféricas, Universidade de São Paulo, Brazil
[c] National Oceanographic Centre, Southampton, United Kingdom

ARTICLE INFO

Keywords:
Rio Grande rise
Submarine geomorphology
Erosional processes
Ferromanganese crusts
Deep-ocean currents

ABSTRACT

The Rio Grande Rise is a submerged plateau that has received increasing interest due to the presence of critical minerals within ferromanganese crusts that partially cover the plateau. The formation, distribution and preservation of the crusts are partially controlled by the hydrodynamic processes that are active around the region. This study was carried out to describe the erosional and depositional processes that have shaped the geomorphology of the Rio Grande Rise in an area where three scientific cruises have recently occurred. Particularly, we investigated the role of ferromanganese crusts in seafloor erosional processes and their interaction with deep ocean currents. For that, we combined the analysis of multibeam bathymetry, sub-bottom profiles and ROV imaging data. Multibeam bathymetry reveals the heterogeneity of submarine morphologies, composed of escarpments, slope scars, submarine canyons, subcircular depressions and erosive channels. Sub-bottom profiles show that deep currents have eroded the plateau flanks, forming contourite drifts only where ferromanganese crusts are absent. ROV images show that current directions are variable, and obstacle scouring occurs widespread. Overall, we show that the presence of ferromanganese crust is crucial in preventing erosion. Lastly, outcrops of basaltic escarpments expose the various characters of volcanic deposits in the Rio Grande Rise, while sediment mass movements including debris flows occur along the scarps. The integrated results shed light on the nature of the seabed erosional processes that affect the region and how the presence of ferromanganese crusts is shaping the morphology of the Rio Grande Rise.

1. Introduction

The Rio Grande Rise (RGR) is a structural high in the western South Atlantic Ocean near Brazil (Fig. 1). The rise formed as a basaltic plateau during the Late Cretaceous through the interaction between the spreading Mid-Atlantic Ridge and the Tristan-Gough hotspot (Camboa and Rabinowitz, 1984; Davidson et al., 2025; Mohriak et al., 2010; O'Connor and Duncan, 1990). Subsequent Eocene volcanism led to the formation of multiple volcanic islands, seamounts, and guyots across the region (Hoyer et al., 2022; Praxedes et al., 2019; Srivastava et al., 2023; Taciro Mandacaru Guerra et al., 2025). The volcanic seamounts and plateaus have originated at or above sea level and have since subsided by hundreds of meters (Coffin and Eldholm, 1994; Praxedes et al., 2019; Silva et al., 2024). The formation of the volcanic plateau established a depth gradient greater than 1000 m, with massive volcanic escarpments along the Cruzeiro do Sul Rift (Camboa and Rabinowitz, 1984). The Cruzeiro do Sul has been described as an aborted Late Cretaceous–Eocene rift formed by extensional tectonics that transects the RGR (Galvão and De Castro, 2017; Mohriak et al., 2010). Atop the volcanic plateau, a dynamic depositional system developed, with varied depositional erosional elements such as large submarine canyons and contourite drift deposits (Jovane et al., 2019; Levchenko et al., 2020a; Levchenko et al., 2020b; Lisniowski et al., 2025; Mohriak et al., 2010; Praxedes et al., 2019).

The RGR is an area of recent economic interest due to the potential resources that occur within ferromanganese crusts, which are widespread across the region (Benites et al., 2023; Montserrat et al., 2019; Jovane et al., 2026). Driven by mineral exploration, multiple studies have been recently developed for the RGR regarding the characterization and estimation of critical metals and rare-earth resources within the

* Corresponding author.
E-mail address: gabrieltagliaro@usp.br (G. Tagliaro).

https://doi.org/10.1016/j.dsr.2026.104709
Received 18 March 2026; Received in revised form 19 May 2026; Accepted 31 May 2026
Available online 1 June 2026

ferromanganese deposits (Benites et al., 2018, 2020, 2021, 2022, 2023; De Matos et al., 2023; Sergipe et al., 2023), as well as the environmental concerns related to potential impacts of future deep-sea mining (Corrêa et al., 2022; Montserrat et al., 2019). Moreover, due to its geographical location and its isolation from continental landmasses, the tectonic sedimentary processes that have shaped the geomorphology of the RGR since its inception have also received considerable scientific attention, with important implications for the understanding of the South Atlantic Cretaceous opening (Hoyer et al., 2022; O'Connor and Duncan, 1990; Sager et al., 2021), and the tectonic evolution of the South Atlantic after its establishment (Hackspacher et al., 2022; Silva et al., 2024; Srivastava et al., 2023). As one of the largest and best-preserved oceanic plateaus in the South Atlantic, the RGR also represents an important analogue for understanding the geological evolution of oceanic plateaus worldwide (Coffin and Eldholm, 1994).

Most depositional features observed in the region have been initiated by gravity-driven flows due to the depth gradient that exists, including the development of extensive and complex submarine canyons on both northern and southern margins of the plateau (Jeck et al., 2019;Jeck et al., 2024; Lisniowski et al., 2025). Ocean circulation then reshapes the seafloor and interacts with the mass-transport deposits across the region (Orletti Del Rey et al., 2024; Rebesco et al., 2014; Souza-Neto et al., 2024). Deep-sea depositional systems are highly dependent on the regional topography, since the interaction between ocean currents and inherited bathymetry may deflect current directions strengthen or weaken its flows (Tagliaro et al., 2021a, 2021b). Given the heterogeneous bathymetry of the RGR, it is expected that current activity throughout the region is highly variable (Souza-Neto et al., 2024), thus we expect that its effect on erosion deposition is varied as well. Quaternary bottom-current activity has been observed near the RGR, associated with the presence of erosional features such as scours, furrows, and depositional contourite drifts ((Jeck et al., 2019;Jeck et al., 2024; Levchenko et al., 2020a;Levchenko et al., 2020b; Lisniowski et al., 2025). In specific, the Antarctic Bottom Water (AABW) influences seafloor and erosion deposition on the deepest regions south of the RGR plateau, and the North Atlantic Deep Water (NADW) affects the seafloor along the deep slopes, while the Upper Circumpolar Deep Water (UCDW) and the Antarctic Intermediate Water (AAIW) affect the seafloor atop the plateaus and on the upper slopes (Fig. 1) (Schlitzer, 2000).

More importantly, extensive hardgrounds of ferromanganese deposits formed atop the RGR plateaus (Benites et al., 2020; Hassan et al., 2024). Development of ferromanganese crusts at the RGR has been associated with the formation of oxygen minimum zones at the nepheloid layers across the region since the Miocene (Benites et al., 2020). Along the seafloor of the RGR, ferromanganese precipitates may be present as fragmented and discontinuous crusts, which partially cover the seafloor; as laterally continuous pavements, where the deposits form extensive hardgrounds that cover the seafloor; or as discrete rounded nodules, which occur as isolated concretions resting on the seabed.

In many settings worldwide, the formation and occurrence of ferromanganese deposits have also been associated with bottom-current activity (Tagliaro et al., 2021a, 2021b; Watkins and Kennett, 1977). The presence of polymetallic nodules and ferromanganese crusts on the seafloor forms a hard substrate that interacts with the depositional system, triggering differential erosion and compaction between the regions with hard and soft-sediment-rich substrates (Watkins and Kennett, 1977). Seabed morphology also plays an important role in controlling the erosive strength of bottom currents and has been shown to affect the distribution and preservation of ferromanganese crusts (Tagliaro et al., 2021b; Yeo et al., 2019). Despite recent contributions that explore selected geomorphic implications of ferromanganese deposits in the RGR (Lisniowski et al., 2025; Orletti Del Rey et al., 2024), the specific role of these deposits in shaping the region's modern geomorphology has yet to be fully demonstrated.

This study discusses the geomorphology produced by the recent depositional and erosional processes in parts of the RGR. In particular, we investigate the role that ferromanganese deposits have on the geomorphological evolution of the Rio Grande Rise. In doing so, we reveal the interactions and feedbacks between hard substrates and deep-sea sediment transport dynamics, which are important for the understanding of regions with abundant deep-sea minerals. A more complete understanding of deep-sea sedimentary dynamics within those regions is crucial for future exploration efforts, including environmental assessment and resource evaluation. For that, we integrated and analyzed data

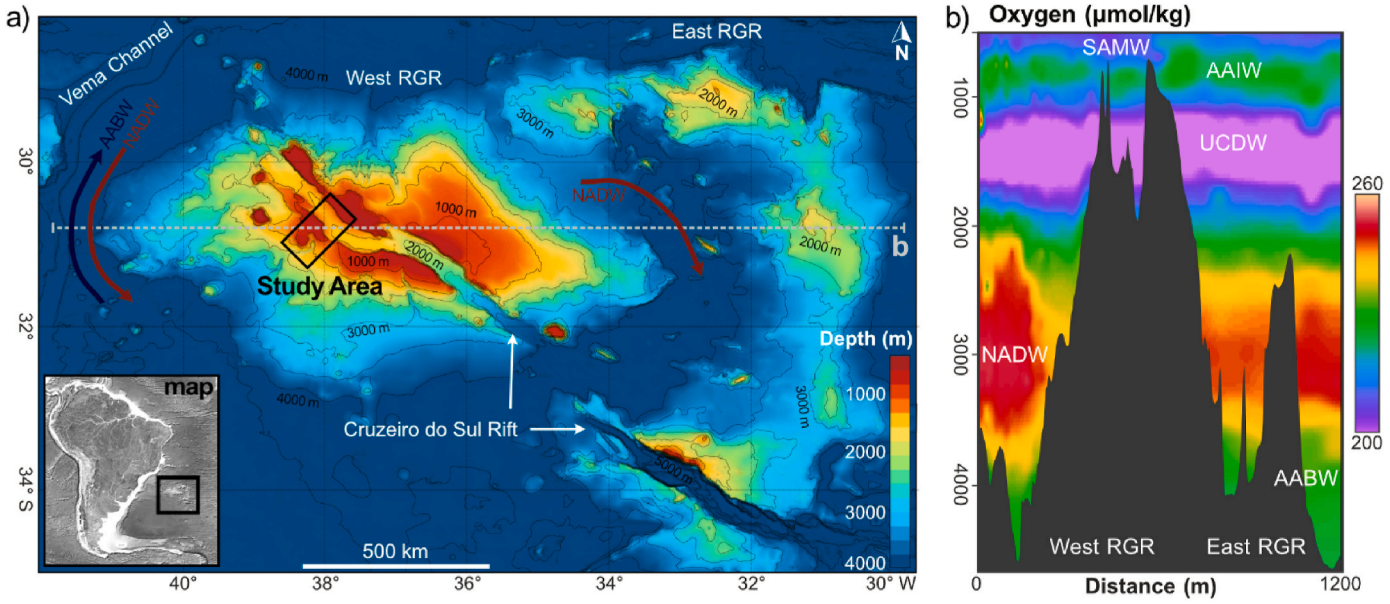

Fig. 1. **(a)** Map of the Rio Grande Rise (RGR) and its main features. The study areas are located on the Western RGR plateaus adjacent to the Cruzeiro do Sul Rift. **(b)** Ocean current action at the seafloor along the RGR is dominated by the North Atlantic Deep Water (NADW), the Upper Circumpolar Deep Water (UCDW) and the Antarctic Intermediate Water (AAIW), while the Antarctic Bottom Water (AABW) is confined within the deeper seafloor regions (>3500 m) and the Sub-Antarctic Mode Water (SAMW) is confined within the top of the RGR plateau. Bathymetry from GEBCO 2020 Grid (GEBCO Compilation Group, 2020) and oxygen water levels from eWOCE (Schlitzer, 2000).

from three research expeditions that occurred along the RGR in the recent past: RGR1 Expedition aboard the N/Oc Alpha Crucis (February of 2018), FAPESP-NERC DY094 Expedition aboard the RRS Discovery (October of 2018), and RGR_VO2023 Expedition aboard the NPqHo Vital de Oliveira (March of 2023). The dataset comprises multibeam bathymetry, sub-bottom profiles and Remotely Operated Vehicle (ROV) seabed images. Our analysis focuses on: (1) the distribution and characteristics of current-driven seafloor erosional and depositional bedforms; (2) the distribution and morphology of hard substrates and their interactions with sediment transport; (3) the aspect of volcanic outcrops and their effects on sediment transport.

2. Geological and oceanographic setting

The Rio Grande Rise (RGR) is an extensive oceanic plateau located in the western South Atlantic, approximately 1200 km east of the Brazilian coast and about 2000 km west of the Mid-Atlantic Ridge (Fig. 1). The RGR formed primarily through increased magmatism during the Coniacian/Santonian (~85-95 Ma), within the context of mantle plume–mid-ocean ridge interactions, particularly the Tristan-Gough plume, which has shaped both the RGR and its conjugate margin, the Walvis Ridge (Davidson et al., 2025; Galvão and De Castro, 2017; Hoyer et al., 2022). As the South Atlantic widened and the RGR drifted away from the Walvis Ridge, a series of volcanic islands transitioned to progressively drowned plateaus, governed by thermal and flexural subsidence (Fodor et al., 1977). In the Eocene, widespread volcanism episodes (~46 Ma) promoted uplift and subaerial exposure of the RGR, followed by thermal subsidence associated with intense erosion and sediment accumulation (Praxedes et al., 2019; Rohde et al., 2013). In this context, prolonged Late Cretaceous–Eocene extensional tectonics favored the development of the Cruzeiro do Sul Rift, part of a NW–SE–trending lineament that dissects the entire RGR (Galvão and De Castro, 2017). At present, the RGR can be divided into western (WRGR) and eastern (ERGR) portions, with the WRGR forming a large elliptical bulge with numerous guyots on its main platform, whereas the ERGR trends north–south, is bounded by fracture zones, and may represent an abandoned spreading center (Fig. 1) (Camboa and Rabinowitz, 1984).

Modern ocean circulation in the RGR region comprises the Antarctic Intermediate Water (AAIW), upper and lower Circumpolar Deep Water (UCDW and LCDW), North Atlantic Deep Water (NADW), and Antarctic Bottom Water (AABW; Fig. 1). On the western portion of RGR, the AAIW is located between the depths 800 and 1200 m, the NADW between 2000 and 3100 m, and the AABW between 3100 and 4100 m (Hogg and Brechner Owens, 1999). Interpretation of water masses on the RGR from oxygen concentration profiles (Koltermann et al., 2011) also found similar range depths of the AAIW (700 to 1100 m), the UCDW (1100 to 1600 m), the NADW (1600 to 3600 m) and the LCDW (3600 to 4500 m), delimiting the AABW to depths >4500 m (Florindo et al., 2003). Close to the RGR, the AAIW is directed to the southwest, the NADW to the southeast, while the AABW flows north along the Vema Channel (Hogg and Brechner Owens, 1999) (Fig. 1). The RGR also acts as a major topographic barrier in the deep ocean thermohaline Atlantic cell, since the depth of the plateau (<3000 m) blocks the north passage of the AABW from the Argentine Basin into the Brazil Basin. Due to the bathymetric blockage, the AABW is then deflected west and passes the RGR through the Vema Channel, one of the most important deepwater passages for the global ocean circulation cell (Hogg and Brechner Owens, 1999; Kaji et al., 2011). The rugged physiography also modulates local hydrodynamics and sediment redistribution, making the RGR a hotspot for M2 internal-tide generation that promotes bottom-intensified currents that drive sectorized deposition, non-deposition, and episodic sediment resuspension (Orletti Del Rey et al., 2024; Souza-Neto et al., 2024, 2026).

One region across the western part of the WRGR was part of this study (Fig. 1). The area crosses the north portion of the Cruzeiro do Sul Rift, covering around 1490 km^2 with water depths between 613 m and 2500 m (Fig. 1). The substrate in this sector is highly heterogeneous, comprising ferromanganese crusts and nodules, phosphorites, ironstones, carbonate rocks, red clays, and unconsolidated sediments, including foraminiferal sands and pteropod shell beds (Benites et al., 2018, 2020, 2022; Lisniowski et al., 2025; Millo et al., 2022; Montserrat et al., 2019; Sergipe et al., 2023; Silva et al., 2024; Srivastava et al., 2023). Ferromanganese crusts are abundant, cobalt-rich, and grow at extremely slow rates (a few mm Ma^{-1}), commonly precipitating on phosphate-rich substrates and carbonate pavements through hydrogenetic and diagenetic processes (Benites et al., 2020, 2023). Two crust generations are recognized: an older, phosphatized generation and a younger hydrogenetic generation formed under oxic conditions and enriched in critical metals (Co, Ni, and Li), with mineralogical differences that include vernadite, goethite, and carbonate fluorapatite (Benites et al., 2020, 2023; De Matos et al., 2023). REY enrichment on RGR ferromanganese deposits is comparable to crusts from the Central (Koschinsky et al., 1997; Xing et al., 2026) and Northwest Pacific (Zhang et al., 2026).

Carbonate substrates, in turn, include facies consistent with the development of a carbonate platform, with the development of lagoonal and reef environments during the Oligocene–Miocene interval of tectonic quiescence, followed by drowning and pelagic sedimentation (Lisniowski et al., 2025; Silva et al., 2024). Carbonate hardgrounds, likely younger, have also been documented in the area, although the mechanisms responsible for their formation remain poorly constrained (Ferraz et al., 2024; Millo et al., 2022). The presence of ironstones associated with geothermal/hydrothermal processes, as well as subcircular depressions possibly related to hypogenic/hydrothermal karstification and collapse, further increases substrate complexity (Benites et al., 2022; Ferraz et al., 2024). This heterogeneity shapes benthic community structure and diversity, with hard substrates supporting sessile suspension feeders (e.g., corals and sponges), whereas softer sediments host diverse invertebrates and detritivores.

3. Methodology

3.1. Sub-bottom profiler

Seismic data was acquired aboard the N/Oc Alpha Crucis in February of 2018 with a Knudsen CHIRP 3260 sub-bottom profiler mounted on the hull of vessel, which operates at 3.5 kHz frequency and 2 kW power. The acquisition software was SoundSuite EchoControl. Data was then converted from a proprietary format to SEGY, and a simple burst noise filter and amplitude correction was applied on RadexPRO. Navigation was provided by an Applanix OceanMaster Inertial Navigation System (IMU) connected to two Trimble GPS antennas. Two subbottom profiling lines that cross the RGR plateau in the study area were selected for this study. For time-depth conversions we use a 1550 m/s seismic velocity for the water column and 1600 m/s for near-seafloor features.

3.2. Multibeam bathymetry

Multibeam bathymetry data was acquired over the RGR during the three expeditions. With the N/Oc Alpha Crucis, acquisition occurred using a Reson Seabat 7160 echosounder operating at 44 kHz with navigation data provided by an Applanix OceanMaster connected to two Trimble GPS antennas (Jovane et al., 2019). Acquisition was achieved using the acquisition module of PDS2000 alongside the Reson Seabat sensor software to modify the settings during surveys (power, pulse length, range, gain, beam width). Survey speed was between 4 and 4.5 knots aligned as much as possible with the prevailing wave direction. Sound Velocity Profiles (SVPs) were collected at least every other day during the survey and at least once per survey to full depth. The Patch Test was carried out in an area north of the Cruzeiro do Sul Rift and applied retrospectively to the data already collected. Data processing was performed using Teledyne PDS 2000 software, following a basic

workflow of spike removal, gridding, and interpolation of no-data cells.

For the operation aboard the NPqHo Vital de Oliveira, acquisition occurred using the Kongsberg SIS software with a Kongsberg EM122 echosounder operating at 12 kHz frequency and with navigation provided by the SeaPath 330 positioning system with two GNSS antennas without differential positioning. Survey speed was between 4 and 4.5 knots. Data processing occurred during acquisition on the software CARIS HIPS and SIPS and postprocessing on the software EIVA Navimodel.

For the operation aboard the RRS Discovery, acquisition occurred with two echosounders: one Kongsberg EM122 multibeam system equipped on the ship hull and one EM2040 equipped on the Autosub 6000 AUV (Autonomous underwater vehicle; Murton et al., 2012). Unfortunately, the EM2040 did not function properly during the expedition and the data acquired was rendered not useful. The EM122 acquisition used the Kongsberg SIS software and was processed in CARIS HIPS AND SIPS. A zero tide was assumed for data processing, and sound velocity data was acquired during two sound velocity dips and incorporated into the data during processing. All multibeam datasets were merged and interpreted together using the software EIVA Navimodel Producer.

3.3. ROV imaging

Seafloor imaging was undertaken during 14 Remotely Operated Vehicle (ROV) dives with the HyBIS (Hydraulic Benthic Interactive Sampler) from the UK National Oceanography Centre aboard the RRS Discovery in October of 2018. HyBIS is a ROV capable of reaching 6000 m of depth, controlled by a fibre optic cable connected to the ship, and equipped with two Super Scorpio HD cameras and one Sony HDR-CX560V camera (Murton et al., 2012). HyBIS dive objectives were to survey and sample the areas of high interest based on the analysis of the multibeam data. Depth range of the survey occurred from 620 m to 1480 m. A total of 5305 GB of data was recorded, including 50 h of video recordings and 13350 images. Interpretation of ROV data occurred via the visual analysis of all video recordings post-survey, with the objective of identifying and interpreting the main geomorphological and seabed erosional structures recorded in the data.

4. Results

4.1. Seismic expression of seafloor features

Subbottom profiling data show that the RGR plateau at the studied area is marked by a high-amplitude low-dipping seafloor reflector atop the plateau, bounded by channels at both southern and northern flanks (Fig. 2a). The channels occur at ~900 m water depths on the northern side of the western plateau and at ~1000 m water depths on its southern side (Fig. 2a). Channels at the western plateau are up to 100 ms two-way travel time (TWT) deep (~80 m) and up to 3 km wide (Fig. 2a). Seismic penetration is poor atop the plateau, but it improves adjacent to the channels, as we can observe subsurface reflections parallel to the seabed, particularly at the eastern Plateau where reflections are embedded within a transparent seismic facies (Fig. 2b). Mounded seafloor morphologies occur downward from the erosional channels, up to 4 km in width (but probably larger as the morphology continues out of data limits) and up to 100 ms (~80 m) in thickness (Fig. 2a). On the eastern plateau, a zone of no-erosion and no-deposition (i.e., moat) occurs upslope from to the mounded morphology, with 2 km of width (Fig. 2b).

4.2. Bathymetric morphologies

Multibeam bathymetry demonstrates the presence of multiple features along and around the submarine plateaus, with the presence of submarine canyons and scars, seafloor channels and terraces, dunes, scours and depressions (Fig. 3). Several subcircular to circular depressions ranging between 50=90 m in depth and 230-530 m in diameter are identified atop the westernmost portion of the plateau, south of the Cruzeiro do Sul rift (Fig. 3a). These depressions have flat bottom smooth-seafloor edges. The scarp walls of the plateaus south and north of the Cruzeiro do Sul rift are the steepest morphologies of the region (Fig. 3b 3c). The southwest-facing escarpment is 500 m high with a steep gradient (Fig. 3b), whereas the northwest-facing escarpment is up to 600 m high, but it shows a lower gradient in comparison to the southern wall, with a smoothed seafloor character (Fig. 3c). A marine terrace is observed atop the northern plateau, up to 70 m in height (Fig. 3b). The

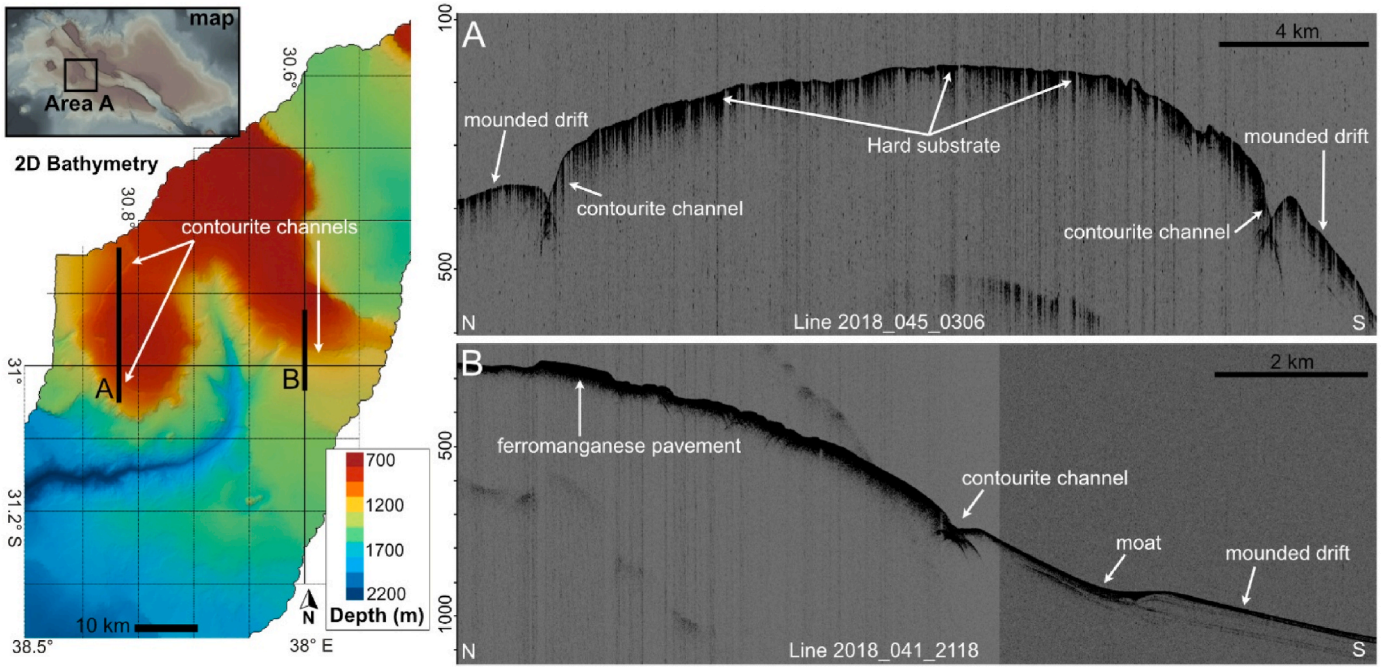

Fig. 2. Sub-bottom profiles on the edges of the plateaus of the study area. The sections show high-impedance seafloor reflections atop the plateau where ferromanganese crusts are present, while contourite drifts (i.e., contourite channels, moats mounded drifts) are active in the northern and southern flanks of the plateau. For contour lines on the map see Fig. 4.

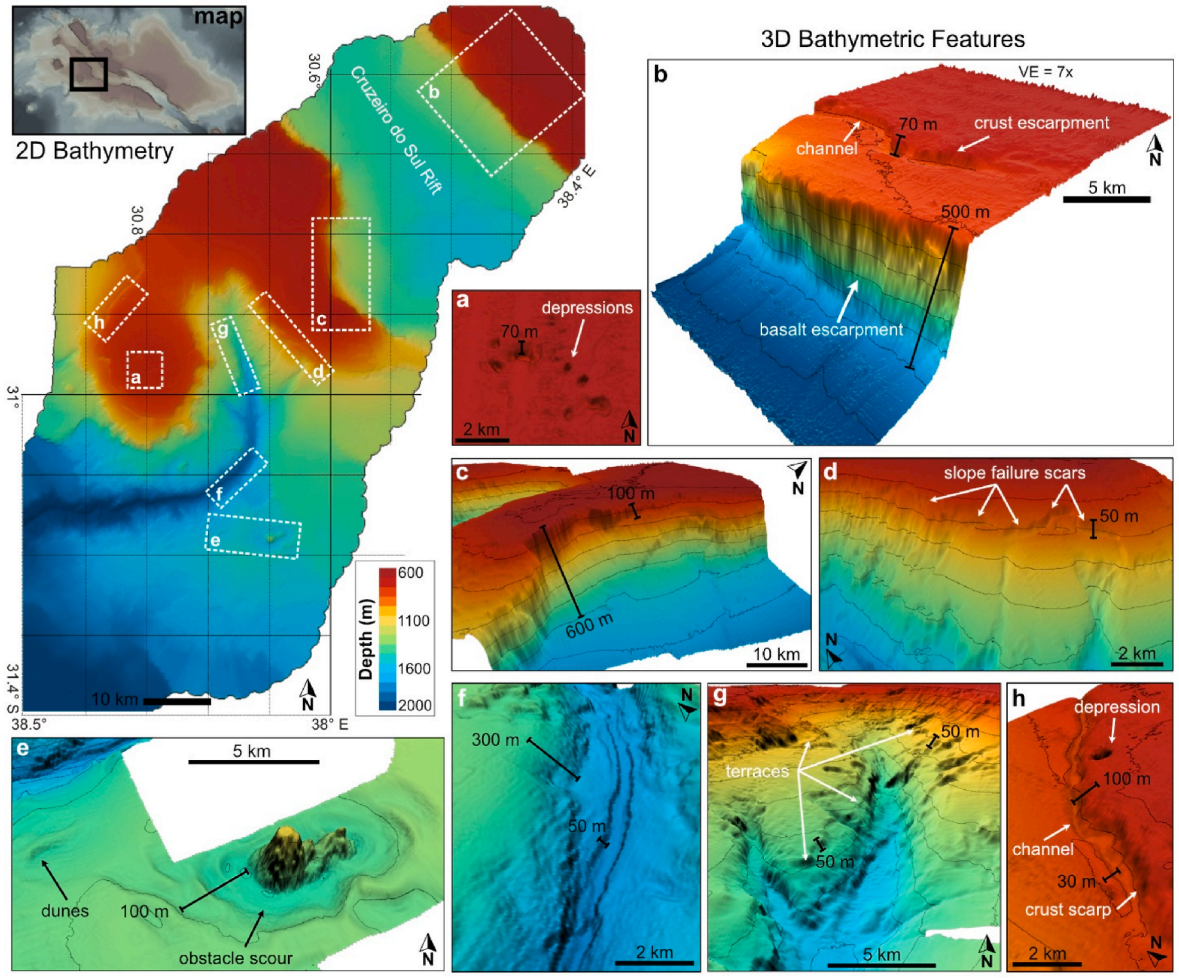

Fig. 3. 2D Bathymetry of study area and 3D images of the main geomorphological features observed. Black lines at the 3D images represent height distance while the scale bar represents horizontal distance. **(a)** Large subcircular depressions in the center of the plateau. **(b)** The region north of the Cruzeiro do Sul Rift is marked by a high escarpment composed of basaltic outcrops. Atop the plateau a cliff develops, formed by ferromanganese crusts with an erosional channel at its bottom. **(c)** On the southern side of the rift, a high escarpment is present, with step-stairs cliffs formed atop the plateau. **(d)** Slope failure scars at different levels of development occur on the slope within the valley. **(e)** Evidence for strong current action is observed with the formation of seafloor dunes and obstacle scour around a submerged seamount. **(f)** The active channel of the canyon shows channel avulsion, with **(g)** multiple terraces formed near the canyon head. **(h)** The erosional channel parallel at the bottom of a hard-substrate scarp.

seafloor character above the terrace is notably more rugged than below the terrace (Fig. 3b). On the southern wall, a marine terrace is also observed above the scarp, up to 100 m in height (Fig. 3c).

On the other side of the southern plateau towards the valley, slope scars are observed across the south-facing slopes (Fig. 3d). These submarine scars occur widespread along this southern flank of the plateau, forming cliffs up to 50 m height (Fig. 3d). On the deepest part of the region, seafloor scouring and dunes are observed around a volcanic hill (Fig. 3e). Obstacle scour generated a 100 m deep depression around the seamount (Fig. 3e). Wave-shaped seafloor morphologies are also observed across this region, with the presence of multiple dunes with average reliefs of 30 m (Fig. 3e).

A large, 64 km long and up to 13 km wide, submarine canyon is present in the central and deeper part of the region, between depths of 1000-2500 m and with an incised depth of up to 500 m (Fig. 3f and g). The main active channel inside the canyon is up to 500 m wide and up to 50 m deep relative to channel banks (Fig. 3f). The submarine canyon is asymmetric, with the eastern edge showing a higher gradient than the western edge (Fig. 3g). Within the canyon, three terrace surfaces can be distinguished, each with ~50 m high cliffs (Fig. 3g). The canyon has two main branches, one at each flank of the main axis, with the presence of an active seafloor channel on the eastern branch. Headward erosion is observed at both canyon branches and along the main axis, connected with slope scars at some regions (as in Fig. 3d). Overall, canyon morphology changes downslope from a marked incised V-shaped towards a broader U-shape at ~2000 m depths (Fig. 3).

Seafloor channels parallel to the isobaths occur atop both northern and southern plateaus but are particularly well-defined on the northern plateau (Fig. 3b) and along the western edge of the southern plateau (Fig. 3h). These channels occur flanking the terrace scarps, with sinuous morphologies (Fig. 3h) and reach up to 300 m wide and up to 30 m of incised depth (Fig. 3b h). Another occurrence of a flat-bottom seafloor circular depression is observed near this western seafloor channel, with 500 m of diameter (Fig. 3h).

4.3. *ROV-imaged seabed features*

4.3.1. *Ferromanganese nodules and crusts*

ROV dives in the study area reveal the diverse and distinct seabed morphologies that form from the presence of ferromanganese nodules and crusts on the seafloor. Ferromanganese nodules mixed with basaltic clasts occur along the sandy-rich seafloor, on where the abundance of nodules is insufficient to completely cover the seafloor (Fig. 4a). In some areas we also observe sub-circular arrangements of nodules, resulting

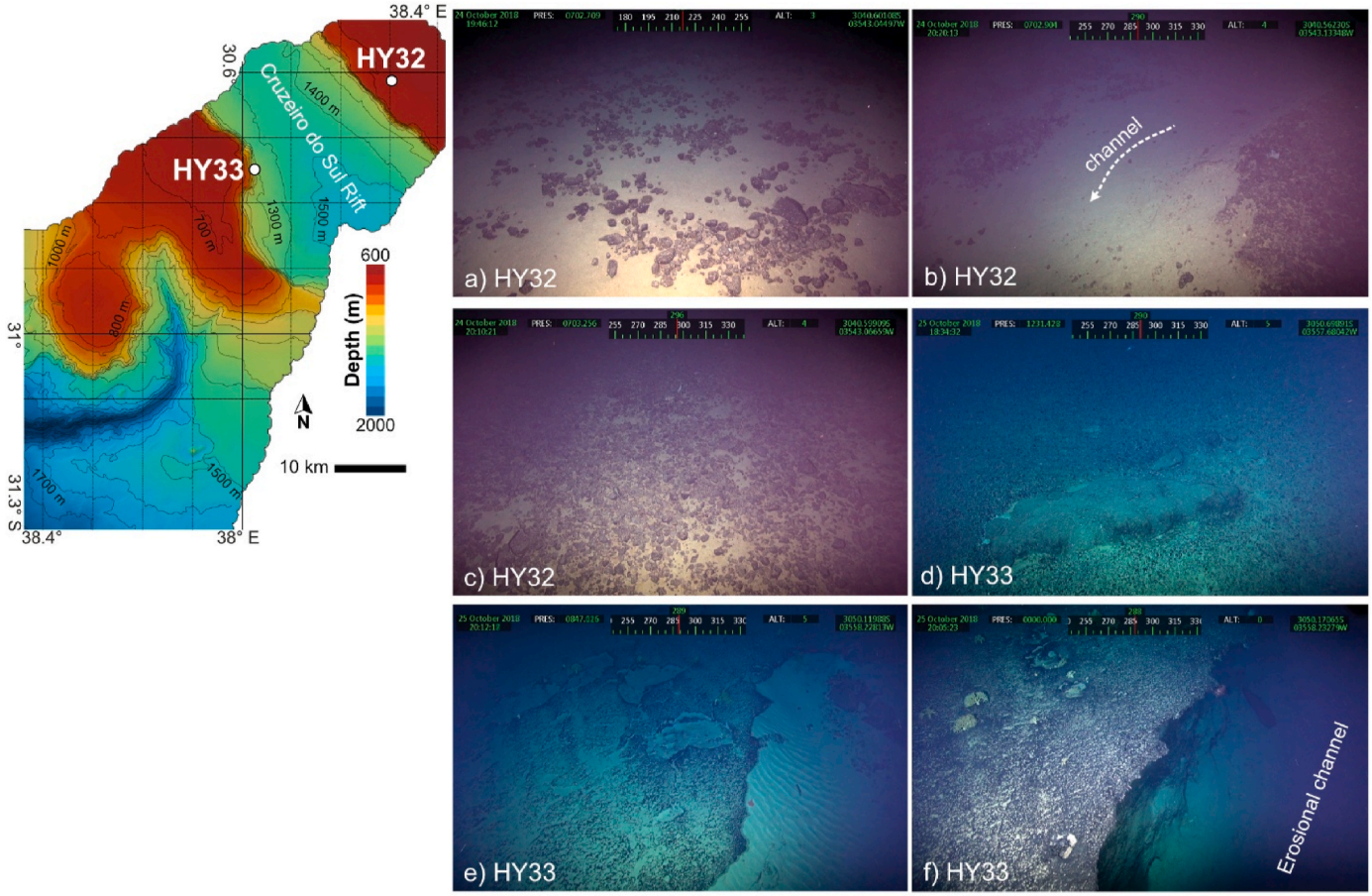

Fig. 4. ROV imagery showing the interactions between ferromanganese crusts, basaltic clasts, and sediments along the RGR seafloor (ROV stations HY32-33). **(a–c)** Eroded dispersed coarse-grained basalt and crust fragments. The distribution of nodules and pavements ranges from **(a)** sparse to **(b)** dense, **(c)** to complete coverage, with the **(b)** hard substrate preventing sediment erosion. **(d)** A region with a carbonate hardground along the seafloor. **(e)** The presence of pavements hinders seafloor erosion, forming step-like terraces and **(f)** cliff outcrops that are being eroded at their bases by current processes. Sediment winnowing prevents accumulation atop the ferromanganese pavements in some regions **(f)**.

from the distribution of gravel and cobble-sized nodules and basaltic clasts on the sandy seafloor (Fig. 4a). In areas where nodules and crusts are less present, we observe the prevalence of erosional features such as channels and scarps (Fig. 4b). The southern plateau is marked by a high concentration of ferromanganese nodules and basaltic fragments that nearly cover the seafloor (Fig. 4c), which also occur around basaltic outcrops (Fig. 4d). Sharp boundaries between hard pavements and adjacent soft sediments are observed, with exposure or accumulation of sandy substrate where the hard cover is discontinuous or absent (Fig. 4e). In some regions, that hard boundary can represent meter-scale terraces escarpments (Fig. 4f).

4.3.2. *Current-driven seabed features*

ROV dives HY33 and HY37 show the variety of seafloor bedforms present at the boundary between the Cruzeiro do Sul Rift and the southern plateau (Fig. 5). At dive HY33, we observe sinuous to short-crested catenary connected ripples and disconnected linguoid lunate ripples (Fig. 5a). Within the same region, silt/sand/gravel lineations and obstacle scouring are also observed around ferromanganese nodules and fragments (Fig. 5b). Dive HY37 shows the presence of long-crested straight to sinuous ripples (Fig. 5c), as well as long-crested connected to disconnected sinuous ripples (Fig. 5d). Dive HY37 is also marked by the presence of erosional features such as sand/gravel lineations, crag and tails, and comet obstacle scours around ferromanganese fragments (Fig. 5e). Moreover, channels occur adjacent to basaltic outcrops at Dive HY37 (Fig. 5f). Ripple thickness varies, with the thickest crests observed within the longitudinal straight ripples of Fig. 5c. Current directions are inferred from the regional distribution of stoss-side and lee-side orientations and are marked heterogenous even across a couple of meters (Fig. 5). Flow direction across the region is therefore highly variable, and all bedforms identified form within a lower flow regime (<0.5 m/s).

4.3.3. *Rock escarpments*

The expression and character of rock outcrops along the RGR are markedly heterogenous, as shown in ROV Dives HY31, HY33, HY34, HY35, and HY42 (Fig. 6). While the main rock component along the region is the volcanic basaltic rocks, volcaniclastic rocks and well-cemented calcareous rocks were also observed. At the northern plateau at Dive HY42, massive dark gray basalts represent the main outcrops within the Cruzeiro do Sul Rift walls (Fig. 6a). At the southern edge of the Cruzeiro do Sul Rift (HY34), the rift wall is marked by the presence of basaltic columnar jointing structures (Fig. 6b). Moreover, channelized debris and mud gravity-flows flowing down the plateau and into the deep rift region can also be observed throughout the rift wall at Dive HY33 (Fig. 6c), overlying massive volcanic outcrops of the Cruzeiro do Sul Rift. Sediment and debris then accumulate towards the bottom of the rift where the slope gradient decreases (Fig. 6d). Volcaniclastic rocks also outcrop within the rift walls at that region (at Dive HY31; Fig. 6e). Finally, Dive HY35 was located on a circular depression at the bottom of the Cruzeiro do Sul Rift. The walls of this depression are formed by a layered, well-cemented calcareous rock (Fig. 6f).

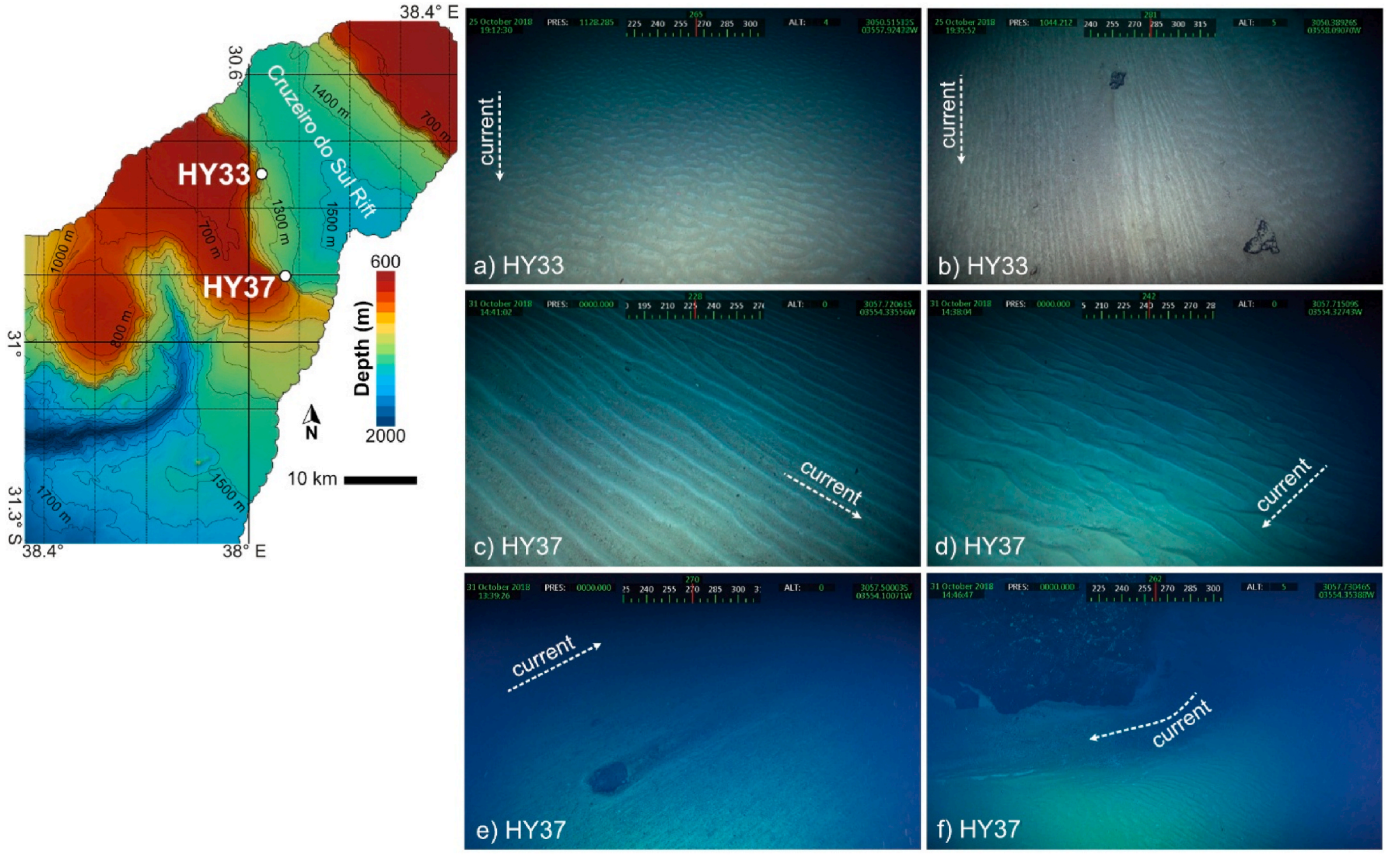

Fig. 5. Current-induced bedforms variability along the Rio Grande Rise (ROV stations HY33 and HY37); **(a)** linguoid disconnected ripples at station HY33; **(b)** sand and gravel lineations and obstacle-scour at HY33; **(c)** longitudinal waves at HY37; **(d)** lunate to sinuous ripples at HY37; **(e)** a large cobble obstacle comet scour; **(f)** an erosional channel around a basalt outcrop. Note that all bedforms observed are associated with low flow velocities. ROV - Remotely Operated Vehicle.

5. Discussion

The studied region exemplifies deep-sea depositional systems far from continental sources, where hemipelagic settling dominates. Sedimentation is strongly controlled by the interaction between deep currents and inherited volcanic topography formed during the Cretaceous–Eocene evolution of the RGR. Additionally, the high relief around the volcanic plateaus (>4000 m depth gradient), promotes widespread gravity-driven slides and channelization, while the presence of authigenic hard substrates (ferromanganese nodules and crusts, and sediments with a carbonate cement) largely affects sediment transport around the region. The role of each erosional depositional process within the RGR is discussed in detail below.

5.1. Contourite drifts and current-driven bedforms

The sediment drifts and adjacent erosional channels observed on sub-bottom profiles are interpreted as contourite drift deposits, based on their morphology and seismic facies (Fig. 2). Although the precise age of horizons cannot be established here, the sediment drifts likely started to form throughout the Pleistocene due to their thin thickness and shallow location within the subsurface, and they remain active in the modern environment (Fig. 2). Based on depth location on the seafloor, contourite drifts identified were formed at the ocean cell between the equatorward-flowing AAIW and the poleward-flowing UCDW (Fig. 1) (Boebel et al., 1997). Such interfaces, where ocean masses of distinct/opposite pathways interact and mix have been widely demonstrated to produce intensified flows that can drive contourite erosion and deposition (Alonso et al., 2023; De Mahiques et al., 2022).

Contourite drifts are only observed along the edges of the plateaus, thus suggesting that the inherited morpho-bathymetric profile around the volcanic plateaus played a critical role in the Quaternary oceanographic setting and sediment transport around the RGR (Tagliaro et al., 2021a). Low penetration and high-amplitude character indicate the presence of a hard substrate atop the plateaus, interpreted as ferromanganese crusts and nodules. Based on the morphology and distribution of contourite features, we interpret that UCDW and AAIW flows are more intense along the plateau slopes, thereby promoting the local formation of large current-induced depositional features. Moreover, the erosional channel along the western edge of the plateau (Fig. 2a and 3h) is slightly shallower than its eastern counterpart (Fig. 2b). The western contourite channel is more erosional (V-shaped geometry), whereas the eastern channel is wider (U-shaped geometry) and contains a non-erosional moat. We interpret these differences in contourite erosion and deposition between the western and eastern edges of the plateau as reflecting stronger currents under the more open western conditions, compared to the more enclosed eastern topography (Figs. 1 and 2). This interpretation is consistent with multiple studies that show that slope morphologies may induce a local intensification of bottom currents (Rebesco et al., 2014; Tagliaro et al., 2021a). Lastly, the association between Quaternary depositional and modern erosional features indicates that seafloor current flows, and therefore current-induced erosion deposition, have remained broadly stable throughout the Quaternary.

An alternative interpretation for the lack of Quaternary contourite features along the plateaus is that the RGR was mostly starved of Quaternary sedimentation, making the development of seismic-scale drift morphologies during this period unlikely. The establishment of non-phosphatized ferromanganese crusts in the Miocene (Benites et al., 2023) likely prevented the remobilization of older strata, diminishing

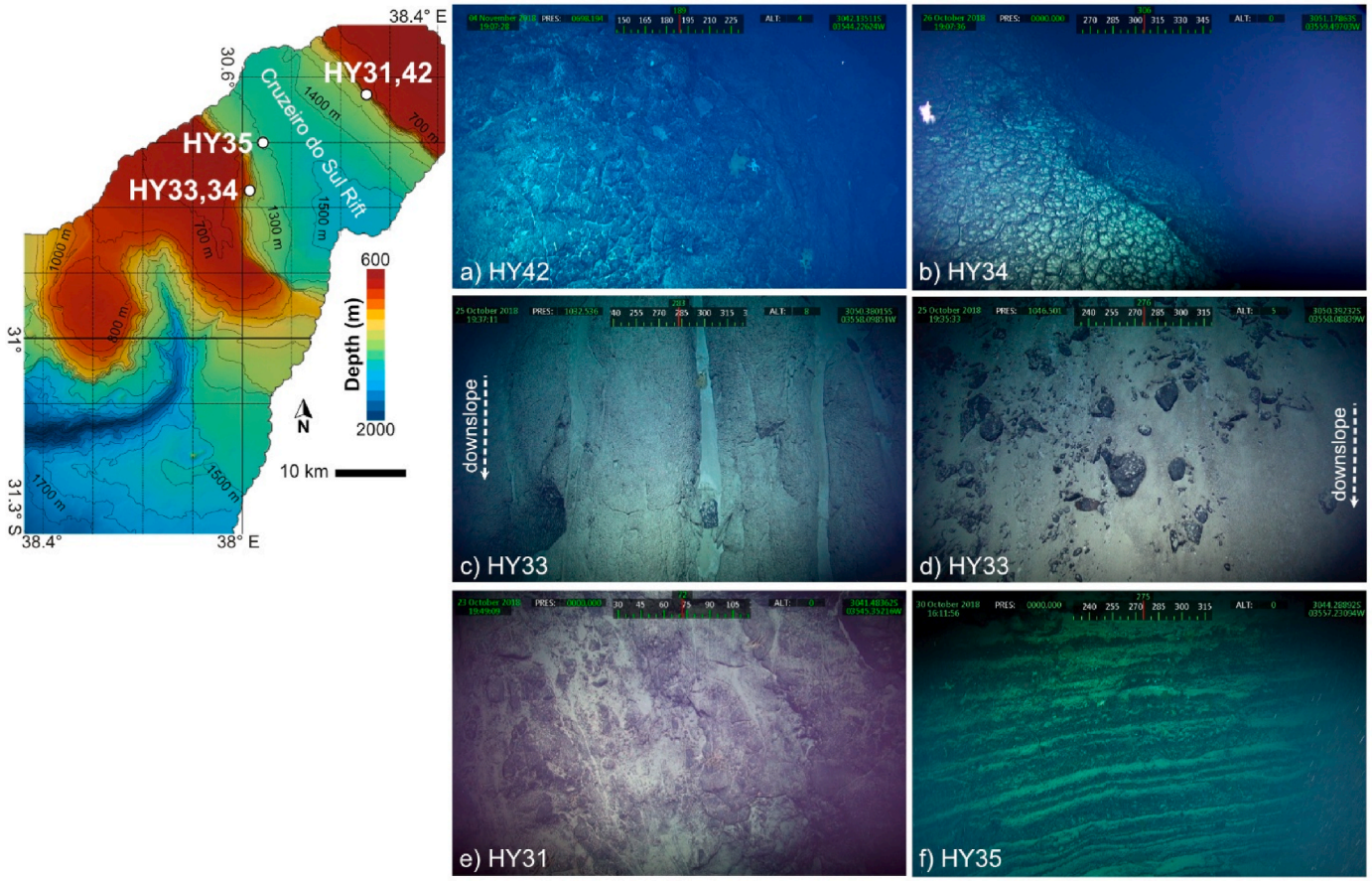

Fig. 6. Main rock outcrops along the RGR (ROV stations HY31, HY34, HY35 and HY42). The basalts of the region outcrop in different ways including as **(a)** massif and with **(b)** columnar joints. Exposed basalts interact with the modern depositional system, overlain by **(c, d)** mass-transport deposits and turbidity currents that move down the slope outcrops. **(e)** Volcaniclastic rocks are also observed within the walls of the Cruzeiro do Sul Rift. **(f)** A seafloor depression within the Cruzeiro do Sul Rift shows calcareous layered outcrops within its walls.

Quaternary sediment supply. Consequently, large depositional features may have developed primarily along slopes, where downslope mass-wasting deposits (hemipelagic sediments, crustal fragments and basalt clasts) are continually accumulated because of current-driven erosion of the plateaus. This interpretation is consistent with the observation that stratigraphic packages overlying the Miocene ferromanganese crusts are thin, typically in the order of centimeters. It also agrees with the low Pleistocene sedimentation rates observed regionally by deep-sea drilling along the Rio Grande Rise (ca. 0.6 cm/ka sedimentation rates at DSDP 516) (Barker et al., 1983). Furthermore, bathymetric evidence indicates that the development of large Quaternary drifts is controlled by sediment supply, since the regionally observed current-driven bedforms form under flow velocities exceeding those required for contourite drift formation (Rebesco et al., 2014) (Fig. 3).

Multibeam bathymetry ROV and images further show the influence of currents on RGR seafloor morphology. First, erosional channels at the base of ferromanganese and carbonate hardground cliffs (Fig. 3b, h, 4f) and within fields of nodules and basaltic fragments (Fig. 4b) occur atop the plateaus (600–700 m depths), under AAIW influence (Fig. 1). We also note the occurrence of lower-flow-regime undulatory ripples atop the plateaus (Fig. 4e), although the region is predominantly characterized by plane beds. On the other hand, ripples and scour bedforms are more common at greater depths (Fig. 5a–f), within the Cruzeiro do Sul Rift walls (1000-1400 m depths; Fig. 5). Bathymetry also shows intense obstacle scouring (Fig. 3e 5f) and larger seafloor dunes at the deeper parts of the region (1200-1600 m depths), under the modern influence of UCDW. Therefore, we interpret that AAIW exerts the main control on seabed erosion atop the plateaus, while UCDW is dominant along the slopes and within the Cruzeiro do Sul rift. Moreover, the effects of the AAIW on the seafloor appear to be pronounced only around topographic obstacles (e.g., cliffs formed by ferromanganese crusts), whereas the effects of the UCDW appear more regionally homogeneous across the deeper domain, with potentially higher and more stable flow velocities.

5.2. *Submarine canyons and gravity-driven erosion*

The large submarine canyon formed a submarine valley where erosion and deposition are dominated by gravity-driven events. Several erosive gullies and slide scars can be observed within both valley walls (Fig. 3). Within this context, sediment supply into the canyon is interpreted to be derived mainly from locally sourced material primarily deposited atop the plateau, including ferromanganese crust, carbonate hardgrounds and basaltic fragments, as well as hemipelagic mud and sands (Benites et al., 2022; Ferraz et al., 2024; Lisniowski et al., 2025). In addition, red clay horizons were documented on the RGR plateaus, interpreted as products of intense subaerial weathering of volcanic rocks formed during the Eocene, prior to subsequent subsidence and submergence (Srivastava et al., 2023). This weathering-derived material may also be locally eroded and remobilized into the modern canyon, likely as a minor component relative to the background hemipelagic supply.

The size and topographic profile of the canyon suggest that it is relatively old, possibly forming just after the onset of the Eocene volcanism that formed the RGR (Barker et al., 1983). Authigenic deposition of ferromanganese crusts atop the plateau in the Miocene (Benites

et al., 2021) likely prevented headward erosion of the canyon-head, which further induced internal incision and an increase in its topographic profile gradient throughout the Cenozoic. Therefore, rates of canyon expansion via headwater erosion probably diminished after the Miocene. The presence of a fully developed channel-levee system further indicates an older age, in which multiple iterations of channel avulsion events have happened since the Eocene (Fig. 3f and g). Moreover, the transversal profile of this canyon reveals an asymmetry with a higher-gradient eastern wall, with depositional marine terraces mostly located on the western wall (Fig. 3g). The terraces are interpreted as levee banks of the main channel-levee system (Fig. 3g). That asymmetry indicates that turbidity currents and channel avulsion are asymmetrically shifted towards east, enhancing erosion of the eastern wall. Although an eastern-flowing current may be in place at that location, thus deflecting turbidity current towards the eastern wall, internal/-autogenic dynamics of the canyon depositional system may outpace current's influence. Internal waves/tides may also have contributed to canyon evolution along the RGR, as the rugged physiography of the Rio Grande Rise enhances internal-tide generation and bottom-current variability (Souza-Neto et al., 2024, 2026). These processes can intensify near-bed shear stress, promoting sediment resuspension and localized erosion along canyon flanks and within the canyon axis, driving asymmetry (Wang et al., 2022).

5.3. Submarine escarpments and the role of crust pavements

Escarpment morphologies within the study area are controlled by the type of substrate in which they occur. Within the Cruzeiro do Sul Rift, escarpments are formed by basalts that are highly resistant to erosion (Type-1 escarpments; Fig. 6). That characteristic results in high gradients with heights above 500 m. At the same time, sediment deposition can smooth such high-gradient escarpment profile, and we observe this pattern in the southern wall of the rift, which has a relatively smoother seafloor and lower gradients (Fig. 3b and c). Given that the northern and southern plateaus have similar ages (Constantino et al., 2017; Rohde et al., 2013), it is possible that the area north of the Cruzeiro do Sul Rift has had overall lower accumulation rates than the southern plateaus, as observed when comparing DSDP 516 and 517 Sites (Barker et al., 1983). The higher seafloor roughness of the northern region further suggests that hemipelagic accumulation above the ferromanganese crusts north of the rift is limited (Fig. 3b). The causes of such distinct regional depositional patterns are unclear, but current patterns may promote more intense erosion within the northern plateau. Similar relationships between limited sediment cover and the occurrence of ferromanganese deposits have been reported elsewhere, including in the South China Sea (Ren et al., 2025).

Besides, smaller escarpments on the plateaus (type-2 escarpments) are capped by ferromanganese pavement, while the underlying substrate comprises older, pre-Miocene carbonate deposits (Fig. 4f) (Benites et al., 2021). A stratified crust-sediment pattern is also observed across the cliff walls. In some areas, although rarer, we also observed escarpments covered by a cemented mix of coralline, hemipelagic sediment, ferromanganese crust/basaltic fragments (as in Fig. 4d) (Benites et al., 2020; Montserrat et al., 2019). Type-2 escarpments are smaller, typically <100 m in height (Fig. 3). Channelization at the base of the escarpments has further increased their gradient profiles through geological time. These escarpments occur only on the borders of both plateaus, suggesting a connection between seafloor erosion and more open/exposed topographies. We interpret that type-2 escarpments only started to develop after the emplacement of the ferromanganese pavements along the summit, which started in the Miocene (ca. 20.1 Ma) (Benites et al., 2023). Therefore, the up to 100 m high escarpments developed after the Miocene, implying long-term erosion rates higher than 5 m/Ma. As described above, type-2 escarpments and associated erosional channels occur within the depth range of AAIW. To conclude, we interpret that the presence of ferromanganese pavements acts as a topographic stabilizer and the main control on RGR modern geomorphology, preventing the erosion of the plateaus but also intensifying seabed erosion locally within type-2 escarpments.

5.4. Carbonate hardgrounds as controls on seafloor erosion

Complementarily, early lithification of younger Quaternary deposits rich in carbonate bioclasts may generate hardgrounds that act as an erosion-resistant cap analogous to the protective effect of ferromanganese pavements, by transforming mobile sediments into firm, more stable surfaces under persistent hydrodynamic forcing (Christ et al., 2015; Lisniowski et al., 2025; Orletti Del Rey et al., 2024; Tucker et al., 2020). On the RGR, winnowing and sediment-bypass regimes associated with bottom currents and internal-tide dynamics can keep surfaces exposed for prolonged periods, which may favor marine-phreatic cementation (Christ et al., 2015; O'Connell and Wallace, 2025; Orletti Del Rey et al., 2024; Souza-Neto et al., 2024; Tucker et al., 2020). The presence of extensive carbonate hardground pavements on the RGR plateaus, polished by bottom-current abrasion (Fig. 4f), supports this interpretation (Immenhauser, 2009). Therefore, by consolidating the seabed and reducing remobilization of the upper sediment column, these hardgrounds may also limit headward erosion and contribute to preserving underlying layers, including shallowly buried ferromanganese pavements and nodules. Where this hardening affects the heterogeneous substrate beneath ferromanganese pavements, it likely reduces erosion and helps preserve the pavement by preventing basal erosion along type-2 escarpments, which would result in their collapses. Comparable cementation-driven stabilization of slope segments has been described on the flanks of seamounts and oceanic islands in the North Atlantic (Tucker et al., 2020). Despite this, early diagenesis and carbonate-hardground formation processes on the RGR remain much less explored than those of ferromanganese crusts (Silva et al., 2024; Tucker et al., 2020; Wright et al., 2025).

6. Conclusion

The Rio Grande Rise is an area of recent interest for deep-sea mineral exploration due to the presence of extensive ferromanganese crusts enriched in critical minerals. At the same time, many gaps in the scientific knowledge of the RGR remain, with important questions still open regarding its geological origin, evolution, and the geomorphological processes that are active in the modern environment. Our results show that the present-day morphology of the RGR is the product of a dynamic interplay between inherited volcanic topography, deep-ocean currents, mass-wasting processes, and the widespread occurrence of ferromanganese crusts and pavements. Together, these factors control sediment transport, erosion, and deposition across the plateau and provide new insights into the evolution of oceanic plateaus more broadly.

A major finding of this study is that ferromanganese crusts are not only an important economic resource, but also a fundamental control on seafloor morphology. By forming extensive hardgrounds, they act as a stabilizing factor on the seafloor and inhibit widespread erosion across the plateaus. In the absence of these crusts, seafloor erosion and canyon-head expansion would likely be significantly more extensive. Two distinct escarpment types were identified, reflecting contrasting origins and ages. Type-1 escarpments are large (>500 m high) features developed along the walls of the Cruzeiro do Sul Rift within volcanic substrates and are interpreted to have formed during the Eocene. Type-2 escarpments are smaller (<100 m high) features that occur atop the plateaus and likely developed after the Miocene emplacement of ferromanganese crusts, where localized scouring around crust pavements progressively evolved into erosional channels.

These findings demonstrate that inherited bathymetry and ferromanganese crusts together exert a first-order control on the geomorphological evolution of the Rio Grande Rise. They further highlight that

ferromanganese crusts should be considered not only as a mineral resource, but also as an integral component of the seafloor system that influences sediment transport and erosion patterns. This improved understanding provides an important framework for assessing the environmental consequences, geohazards, and operational challenges associated with future deep-sea mineral exploration on the Rio Grande Rise and in other regions where ferromanganese crusts occur.

Data statement

The datasets used in this work are available at Mendeley Data Repository at 10.17632/spv6cg9xsj.1. For the ROV data, we have deposited in the repository the ROV dive videos that cover the areas shown in Fig. 4, Fig. 5and Fig. 6. The full ROV dataset analyzed in this study comprises 50 h of video, which far exceeds the size limits of repositories. The additional ROV data can be requested directly from the authors.

CRediT authorship contribution statement

Gabriel Tagliaro: Conceptualization, Data curation, Formal analysis, Investigation, Methodology, Resources, Software, Validation, Visualization, Writing – original draft, Writing – review & editing. **Alexandre Henrique Ferraz:** Conceptualization, Investigation, Writing – original draft, Writing – review & editing. **Raylla Souza Silva:** Conceptualization. **Christian Millo:** Writing – review & editing. **Renata Regina Constantino:** Writing – review & editing. **Bramley J. Murton:** Conceptualization, Data curation, Funding acquisition, Project administration, Resources, Writing – review & editing. **Luigi Jovane:** Conceptualization, Data curation, Funding acquisition, Project administration, Supervision, Writing – review & editing.

Declaration of competing interest

The authors declare that they have no known competing financial interests or personal relationships that could have appeared to influence the work reported in this paper.

7. Acknowledgments

This work has been developed within the framework of two projects: FAPESP/NERC Marine E-Tech (2014/50820-7), and FAPESP-CORE (2016/24946-9) projects. Gabriel Tagliaro was supported by FAPESP post-doctoral grants 2020/08847-6, 2023/14454-5, and CNPQ project 447445/2024-3. Raylla Souza and Luigi Jovane were supported by FAPESP grants 2018/12038-6 and 2016/24946-9, respectively. Alexandre Ferraz and Christian Millo were supported by FAPESP grants 2022/03363-6 and 2022/02847-0, respectively. Murton was supported by Natural Environment Research Council (UK) grant NE/M011186/1 which funded the Marine E-Tech project. The authors also acknowledged the Brazilian Navy, Petróleo Brasileiro S.A. (PETROBRAS), and the Brazilian Oil Regulatory Agency (ANP) for enabling the field campaigns under the logistic cooperation terms. We used ChatGPT (OpenAI) to improve clarity and readability of the manuscript text, which were thoroughly reviewed by the authors, who take full responsibility for the final content.

Data availability

The datasets used are available at Mendeley Data Repository, including ROV videos used for Fig. 4, Fig. 5 andFig. 6. The full ROV dataset analyzed can be requested directly from the authors.
https://data.mendeley.com/datasets/spv6cg9xsj/2

References

Alonso, B., Ercilla, G., Juan, C., López-González, N., Cacho, I., Francés, G., et al., 2023. Contourite stratigraphic models linked to the light intermediate versus dense deep Mediterranean water flow regime variations (Alboran Sea, SW Mediterranean). Mar. Geol. 465, 107147. https://doi.org/10.1016/j.margeo.2023.107147.

Barker, P.F., Carlson, R.L., Johnson, D.A., 1983. Initial Reports of the Deep Sea Drilling Project, 72. U.S. Government Printing Office. https://doi.org/10.2973/dsdp.proc.72.1983, 72.

Benites, M., González, J., Hein, J., Marino, E., Reyes, J., Millo, C., Jovane, L., 2023. Controls on the chemical composition of ferromanganese crusts from deep-water to the summit of the Rio Grande Rise, South Atlantic Ocean. Mar. Geol. 462, 107094. https://doi.org/10.1016/j.margeo.2023.107094.

Benites, M., Hein, J.R., Mizell, K., Blackburn, T., Jovane, L., 2020. Genesis and evolution of Ferromanganese crusts from the summit of Rio Grande rise, Southwest Atlantic Ocean. Minerals 10 (4), 349. https://doi.org/10.3390/min10040349.

Benites, M., Hein, J.R., Mizell, K., Farley, K.A., Treffkorn, J., Jovane, L., 2022. Geochemical insights into formation of enigmatic ironstones from Rio Grande rise, South Atlantic Ocean. Mar. Geol. 444, 106716. https://doi.org/10.1016/j.margeo.2021.106716.

Benites, M., Hein, J.R., Mizell, K., Jovane, L., 2021. Miocene phosphatization of rocks from the summit of Rio Grande Rise, Southwest Atlantic Ocean. Paleoceanogr. Paleoclimatol. https://doi.org/10.1029/2020pa004197.

Benites, M., Millo, C., Hein, J., Nath, B., Murton, B., Galante, D., Jovane, L., 2018. Integrated geochemical and morphological data provide insights into the genesis of Ferromanganese nodules. Minerals 8 (11), 488. https://doi.org/10.3390/min8110488.

Boebel, O., Schmid, C., Zenk, W., 1997. Flow and recirculation of antarctic intermediate water across the Rio Grande rise. J. Geophys. Res., Oceans 102 (C9), 20967–20986. https://doi.org/10.1029/97JC00977.

Camboa, L.A.P., Rabinowitz, P.D., 1984. The evolution of the Rio Grande Rise in the southwest Atlantic Ocean. Mar. Geol. 58 (1–2), 35–58. https://doi.org/10.1016/0025-3227(84)90115-4.

Christ, N., Immenhauser, A., Wood, R.A., Darwich, K., Niedermayr, A., 2015. Petrography and environmental controls on the formation of Phanerozoic marine carbonate hardgrounds. Earth Sci. Rev. 151, 176–226. https://doi.org/10.1016/j.earscirev.2015.10.002.

Coffin, M.F., Eldholm, O., 1994. Large igneous provinces: crustal structure, dimensions, and external consequences. Rev. Geophys. 32 (1), 1–36. https://doi.org/10.1029/93RG02508.

Constantino, R.R., Hackspacher, P.C., Souza, I. A. de, Costa, I.S.L., 2017. Basement structures over Rio Grande Rise from gravity inversion. J. South Am. Earth Sci. 75, 85–91. https://doi.org/10.1016/j.jsames.2017.02.005.

Corrêa, P.V.F., Jovane, L., Murton, B.J., Sumida, P.Y.G., 2022. Benthic megafauna habitats, community structure and environmental drivers at Rio Grande Rise (SW Atlantic). Deep Sea Res. Oceanogr. Res. Pap. 186, 103811. https://doi.org/10.1016/j.dsr.2022.103811.

Davidson, P.C., Koppers, A.A.P., Class, C., Sager, W.W., Heaton, D., 2025. 40Ar/39Ar dating reveals over 30 million years of plume-ridge interaction formed the Rio Grande Rise. Commun. Earth Environ. 6 (1), 588. https://doi.org/10.1038/s43247-025-02572-y.

De Mahiques, M.M., Lobo, F.J., Schattner, U., López-Quirós, A., Rocha, C.B., Dias, R.J.S., et al., 2022. Geomorphological imprint of opposing ocean bottom currents, a case study from the southeastern Brazilian Atlantic margin. Mar. Geol. 444, 106715. https://doi.org/10.1016/j.margeo.2021.106715.

De Matos, C.S., Benites, M., Jovane, L., Ulsen, C., 2023. Chemical-mineralogical characterization of critical elements into ferromanganese crusts. J. Mater. Res. Technol. 25, 5633–5649. https://doi.org/10.1016/j.jmrt.2023.07.021.

Ferraz, A.H., Millo, C., Giannini, P.C.F., Felipe, T.C., Pestilho, A.L.S., Monteiro, L.V.S., et al., 2024. First geological survey and characterisation of a giant depression in carbonate strata at the Rio Grande Rise (southwestern Atlantic). Geomorphology 465, 109406. https://doi.org/10.1016/j.geomorph.2024.109406.

Florindo, F., Bohaty, S.M., Erwin, P.S., Richter, C., Roberts, A.P., Whalen, P.A., Whitehead, J.M., 2003. Magnetobiostratigraphic chronology and palaeoenvironmental history of Cenozoic sequences from ODP sites 1165 and 1166, Prydz Bay, Antarctica. Palaeogeogr. Palaeoclimatol. Palaeoecol. 198 (1–2), 69–100. https://doi.org/10.1016/s0031-0182(03)00395-x.

Fodor, R.V., Husler, J.W., Kumar, N., 1977. Petrology of volcanic rocks from an aseismic rise: implications for the origin of the Rio Grande rise, South Atlantic Ocean. Earth Planet Sci. Lett. 35 (2), 225–233. https://doi.org/10.1016/0012-821X(77)90125-X.

Galvão, I.L.G., De Castro, D.L., 2017. Contribution of global potential field data to the tectonic reconstruction of the Rio Grande Rise in the South Atlantic. Mar. Petrol. Geol. 86, 932–949. https://doi.org/10.1016/j.marpetgeo.2017.06.048.

Hackspacher, P.C., Venancio Da Silva, B., Constantino, R.R., Françoso De Godoy, D., Siqueira Ribeiro, M.C., 2022. Uplift and subsidence of the RGR. In: Meso-Cenozoic Brazilian Offshore Magmatism. Elsevier, pp. 231–256. https://doi.org/10.1016/B978-0-12-823988-9.00002-2.

Hassan, M.B., Koschinsky, A., Da Silva, G.L.X., Dantas, R.C., Kuhn, T., Millo, C., et al., 2024. Magnetization of Ferromanganese crusts: geochemical and magnetic insights from Rio Grande rise and tropic seamount. G-cubed 25 (6). https://doi.org/10.1029/2023GC011210 e2023GC011210.

Hogg, N.G., Brechner Owens, W., 1999. Direct measurement of the deep circulation within the Brazil Basin. Deep Sea Res. Part II Top. Stud. Oceanogr. 46 (1–2), 335–353. https://doi.org/10.1016/S0967-0645(98)00097-6.

Hoyer, P.A., Haase, K.M., Regelous, M., O'Connor, J.M., Homrighausen, S., Geissler, W. H., Jokat, W., 2022. Mantle plume and rift-related volcanism during the evolution of

the Rio Grande Rise. Commun. Earth Environ. 3 (1), 18. https://doi.org/10.1038/s43247-022-00349-1.
Immenhauser, A., 2009. Estimating palaeo-water depth from the physical rock record. Earth Sci. Rev. 96 (1–2), 107–139. https://doi.org/10.1016/j.earscirev.2009.06.003.
Jeck, Izabel K., Alberoni, A.A.L., Torres, L.C., Zalán, P.V., 2019. The Santa Catarina Plateau and the nature of its basement. Geo Mar. Lett. 1–12. https://doi.org/10.1007/s00367-019-00585-z.
Jeck, Izabel King, Silveira, I.C.A., da Jr., A.G.F., Brazil, N., 2024. Morphology and sedimentary processes in Santa Catarina Plateau and Vema Channel, Brazil. Geo Mar. Lett. 44 (4), 15. https://doi.org/10.1007/s00367-024-00777-2.
Jovane, L., Hein, J.R., Yeo, I.A., Benites, M., Bergo, N.M., Corrêa, P.V.F., et al., 2019. Multidisciplinary scientific cruise to the Rio Grande rise. Front. Mar. Sci. 6, 252. https://doi.org/10.3389/fmars.2019.00252.
Jovane, L., Ulsen, C., Galante, D., Bernardini, S., Bergo, N.M., Braga, E.D.S., Brandini, F. P., Carrion, R., De Castro, D.L., Constantino, R.R., Hassan, M.B., Janasi, V.D.A., Jeck, I.K., De Oliveira Junior, L., Couto Junior, M.A., Lima, F.A., Marques, S., Massola, G.M., Mestre, N.C.C., Mohriak, W., Monlevade, E.F., De Oliveira, C.C., Pellizari, V.H., Portes, M.C., Praxedes, A.G.P., Rodrigues, F., Rodrigues, L.C.V., González Sanz, F.J., Da Silveira, I.C.A., Soto, J.M.R., Souza-Neto, P.W., Sumida, P.Y. G., Tagliaro, G.T., Da Silva, S.T., Turra, A., Santos, R.V., Yamamoto, M., Mello, S.L. M., 2026. The Rio Grande rise: current knowledge and future frontiers for deep-sea science, mineral resources and governance. Minerals 16, 418. https://doi.org/10.3390/min16040418.
Kaji, A.O., Guerra, J.V., Fernandes, A.M., Oliveira, R.F.D., Silva, C.G., Reis, A.T.D., 2011. Potential de transporte sedimentar pelas correntes de fundo na região do Canal de Vema (Atlântico Sul). Rev. Bras. Geofís. 29 (2), 385–400. https://doi.org/10.1590/S0102-261X2011000200013.
Koltermann, K.P., Gouretski, V.V., Jancke, K., Sparrow, M., Chapman, P., Gould, J., 2011. Atlantic Ocean. National Oceanography Center, Southampton.
Koschinsky, A., Stascheit, A., Bau, M., Halbach, P., 1997. Effects of phosphatization on the geochemical and mineralogical composition of marine ferromanganese crusts. Geochem. Cosmochim. Acta 61 (19), 4079–4094.
Levchenko, O.V., Borisov, D.G., Libina, N.V., 2020a. Contourites and Gravitites on the Rio Grande Rise, Southwest Atlantic Ocean (Seismoacoustic Data). Lithol. Miner. Resour. 55 (3), 165–176. https://doi.org/10.1134/S0024490220030037.
Levchenko, O.V., Lobkovskii, L.I., Borisov, D.G., Libina, N.V., 2020b. Seismic evidences of contourites on the Rio Grande rise, Southwest Atlantic. Dokl. Earth Sci. 490 (1), 40–45. https://doi.org/10.1134/S1028334X20010043.
Lisniowski, M.A., Lopes, V.H.R., Frazão, E.P., Motta Neto, C.C., Harlamov, V., Ayres Neto, A., 2025. Mapping potential benthic habitats of the Rio Grande Rise, SW Atlantic. Deep Sea Res. Oceanogr. Res. Pap. 226, 104619. https://doi.org/10.1016/j.dsr.2025.104619.
Millo, C., Vieira Do Nascimento E Silva, M.H., De Mello, R.M., Leckie, R.M., Benites, M., Fonseca Giannini, P.C., et al., 2022. Discovery of enigmatic toroidal carbonate concretions on the Rio Grande Rise (Southwestern Atlantic Ocean). Mar. Geol. 443, 106665. https://doi.org/10.1016/j.margeo.2021.106665.
Mohriak, W.U., Nóbrega, M., Odegard, M.E., Gomes, B.S., Dickson, W.G., 2010. Geological and geophysical interpretation of the Rio Grande Rise, south-eastern Brazilian margin: extensional tectonics and rifting of continental and oceanic crusts. Pet. Geosci. 16 (3), 231–245. https://doi.org/10.1144/1354-079309-910.
Montserrat, F., Guilhon, M., Corrêa, P.V.F., Bergo, N.M., Signori, C.N., Tura, P.M., et al., 2019. Deep-sea mining on the Rio Grande Rise (Southwestern Atlantic): a review on environmental baseline, ecosystem services and potential impacts. Deep Sea Res. Oceanogr. Res. Pap. 145, 31–58. https://doi.org/10.1016/j.dsr.2018.12.007.
Murton, B.J., Huhnerbach, V., Garrard, J., 2012. HyBIS: a new concept in versatile, 6000-m rated robotic underwater vehicles. In: Roberts, G.N., Sutton, R. (Eds.), Further Advances in Unmanned Marine Vehicles. Institution of Engineering and Technology, pp. 45–67. https://doi.org/10.1049/PBCE077E_ch3.
O'Connell, B., Wallace, M.W., 2025. The palaeoenvironmental and biological significance of marine carbonate depositional surfaces. Geological Society, London, Special Publications 556 (1), 177–201. https://doi.org/10.1144/SP556-2024-90.
O'Connor, J.M., Duncan, R.A., 1990. Evolution of the walvis ridge-rio grande rise hot spot System: implications for African and South American plate motions over plumes. J. Geophys. Res. Solid Earth 95 (B11), 17475–17502. https://doi.org/10.1029/JB095iB11p17475.
Orletti Del Rey, G., Souza-Neto, P.W., Cruz Vieira, L., Del Rey, A.C., Ayres Neto, A., Lisniowski, M.A., Ventura Santos, R., 2024. Exploring subaqueous bedforms and its relation to hydrodynamics in the Rio Grande Rise, Southwestern Atlantic. Mar. Geol. 478, 107434. https://doi.org/10.1016/j.margeo.2024.107434.
Praxedes, A.G.P., Castro, D. L. de, Torres, L.C., Gambôa, L.A.P., Hackspacher, P.C., 2019. New insights of the tectonic and sedimentary evolution of the Rio Grande Rise, South Atlantic Ocean. Mar. Petrol. Geol. 110, 335–346. https://doi.org/10.1016/j.marpetgeo.2019.07.035.
Rebesco, M., Hernández-Molina, J.F., Rooij, D., Wåhlin, A., 2014. Contourites and associated sediments controlled by deep-water circulation processes: State-of-the-art and future considerations. Mar. Geol. 352, 111–154. https://doi.org/10.1016/j.margeo.2014.03.011.
Ren, J.B., Yang, Y., Zhang, L.X., Zhang, L.M., Deng, Y.N., Ren, Y.Z., Hong, S., Ma, J.F., Deng, X.Z., Yu, M., Sun, Z., He, G.W., 2025. Discovery of dense Ferromanganese nodules in the central Basin of the South China Sea: insights into metallogenesis processes and resource potential. Geophys. Res. Lett. 52.
Rohde, J.K., Van Den Bogaard, P., Hoernle, K., Hauff, F., Werner, R., 2013. Evidence for an age progression along the Tristan-Gough volcanic track from new 40Ar/39Ar ages on phenocryst phases. Tectonophysics 604, 60–71. https://doi.org/10.1016/j.tecto.2012.08.026.
Sager, W.W., Thoram, S., Engfer, D.W., Koppers, A.A.P., Class, C., 2021. Late Cretaceous Ridge reorganization, microplate Formation, and the evolution of the Rio Grande rise – walvis Ridge hot spot twins, South Atlantic Ocean. G-cubed. https://doi.org/10.1029/2020gc009390.
Schlitzer, R., 2000. Electronic atlas of WOCE hydrographic and tracer data now available. EOS Trans. Am. Geophys. Union 81 (5). https://doi.org/10.1029/00eo00028, 45–45.
Sergipe, P.P., Louro, V., Marangoni, Y.R., De Moura, D.S., Jovane, L., 2023. A study of volcanic rocks and ferromanganese crusts through marine geophysical methods integration in the north portion of Cruzeiro do Sul Rift in the Rio Grande Rise. Front. Mar. Sci. 10, 1093108. https://doi.org/10.3389/fmars.2023.1093108.
Silva, R.O., Leite, M.G.P., Krahl, G., Rudnitzki, I., Santos Soares, I.A., Souza, M.L., et al., 2024. Neogene isolated carbonate platform of the Rio Grande rise (southwest Atlantic ocean). J. South Am. Earth Sci. 145, 105044. https://doi.org/10.1016/j.jsames.2024.105044.
Souza-Neto, P.W.M., Da Silveira, I.C.A., Rocha, C.B., Lazaneo, C.Z., Calil, P.H.R., 2024. The Rio Grande Rise circulation: dynamics of an internal tide conversion hotspot in the Southwestern Atlantic. Prog. Oceanogr. 224, 103264. https://doi.org/10.1016/j.pocean.2024.103264.
Souza-Neto, P.W.M., Hassan, M.B., Amorim, J.P.M., Borges-Silva, M., Rocha, C.B., Da Silveira, I.C.A., 2026. Hydrodynamic control over shallow ferromanganese crust deposits in the West Rio Grande Rise. Reg. Stud. Mar. Sci. 95, 104833. https://doi.org/10.1016/j.rsma.2026.104833.
Srivastava, P., Murton, B.J., Sant'Anna, L.G., Florindo, F., Hassan, M.B., Taciro Mandacaru Guerra, J., et al., 2023. Red clays indicate sub-aerial exposure of the Rio Grande Rise during the Eocene volcanic episode. Sci. Rep. 13 (1), 19092. https://doi.org/10.1038/s41598-023-46273-y.
Taciro Mandacaru Guerra, J., De Assis Janasi, V., Srivastava, P., Stipp Basei, M.A., Luvizotto, G.L., Jovane, L., 2025. Petrology of the Eocene alkaline volcanism from the western Rio Grande Rise, South Atlantic Ocean. Front. Earth Sci. 12, 1527863. https://doi.org/10.3389/feart.2024.1527863.
Tagliaro, G., Wainman, C.C., Fulthorpe, C.S., 2021a. Inherited morphobathymetric controls over contourite drift deposition: a case study from the late Cenozoic Mentelle Basin, Australia. Interpretation 9 (3), T637–T652. https://doi.org/10.1190/INT-2020-0131.1.
Tagliaro, Gabriel, Fulthorpe, C.S., Watkins, D.K., Vleeschouwer, D.D., Brumsack, H., Bogus, K., Lavier, L.L., 2021b. Late miocene-pliocene vigorous Deep-Sea circulation in the Southeast Indian Ocean: paleoceanographic and tectonic implications. Paleoceanogr. Paleoclimatol. https://doi.org/10.1029/2021pa004303.
Tucker, M.E., Carey, S.N., Sparks, R.S.J., Stinton, A., Leng, M., Robinson, L., et al., 2020. Carbonate crusts around volcanic islands: composition, origin and their significance in slope stability. Mar. Geol. 429, 106320. https://doi.org/10.1016/j.margeo.2020.106320.
Wang, X., Cai, F., Sun, Z., Li, Q., Li, A., Sun, Y., et al., 2022. Tectonic and oceanographic controls on the slope-confined dendritic canyon system in the Dongsha Slope, South China Sea. Geomorphology 410, 108285. https://doi.org/10.1016/j.geomorph.2022.108285.
Watkins, N.D., Kennett, J.P., 1977. Erosion of deep-sea sediments in the Southern Ocean between longitudes 70°E and 190°E and contrasts in manganese nodule development. Mar. Geol. 23 (1–2), 103–111. https://doi.org/10.1016/0025-3227(77)90084-6.
Wright, V.P., Nohl, T., Munnecke, A., 2025. Bedding and bedding surfaces in carbonate and mixed carbonate–siliciclastic successions part 2: processes, identification and implications of diagenetic bedding. Geological Society, London, Special Publications 556 (1), 155–175. https://doi.org/10.1144/SP556-2024-94.
Xing, J.Q., Ren, J.B., Xian, H.Y., et al., 2026. Biogeochemical cycling controls REY enrichment in marine phosphates. Sci. China Earth Sci. https://www.sciengine.com/SCES/doi/10.1007/s11430-025-1893-0.
Yeo, I.A., Howarth, S.A., Spearman, J., Cooper, A., Crossouard, N., Taylor, J., et al., 2019. Distribution of and hydrographic controls on ferromanganese crusts: Tropic Seamount, Atlantic. Ore Geol. Rev. 114, 103131. https://doi.org/10.1016/j.oregeorev.2019.103131.
Zhang, L.M., Ren, J.B., Chen, H.J., Wang, H.Z., Sun, Z., Yang, Y., Zhang, H.D., Wei, Z.Q., Zhang, L.X., Ren, Y.Z., He, G.W., 2026. Fe-Mn crust δ98Mo decline records tectonic forcing on marine oxide sink reduction during the early eocene-early Oligocene. Geophys. Res. Lett. 53 e2025GL120782.